

---

# OmniGF: A Dual-Branch Vision-Language Framework for Unified Gaze Following

---

Qiaomu Miao<sup>1</sup> Haoyu Wu<sup>1</sup> Jingyi Xu<sup>1</sup> Minh Hoai<sup>2</sup> Dimitris Samaras<sup>1</sup>  
<sup>1</sup>Stony Brook University <sup>2</sup>The University of Adelaide

## Abstract

Understanding human gaze behavior is essential for complex scene comprehension and human-computer interaction. Traditional gaze following models are typically restricted to pure spatial localization, lacking the high-level capacity to reason about semantic targets or complex social contexts. Furthermore, these models often process individuals sequentially, requiring redundant computations over the same scene image for multi-person inference. While recent Vision-Language Models (VLMs) offer the exceptional semantic reasoning needed to address gaze-related semantic tasks, their reliance on discrete text generation inherently limits precision in continuous spatial tasks like gaze localization. To bridge this gap, we propose OmniGF, a unified vision-language framework that adapts foundational VLMs for highly scalable multi-person gaze reasoning. The model adopts a dual-branch decoding strategy: a structured language branch generates discrete reasoning states, while a continuous spatial branch directly taps into the VLM’s dense hidden states. Supervising these extracted representations with high-resolution gaze target heatmaps effectively overcomes the spatial bottleneck of text-only coordinate generation. Furthermore, to explicitly ground the model in multi-person scenes, we augment the input with head embeddings encoded from cropped head images, providing fine-grained appearance and orientation cues for all individuals simultaneously. By modeling all individuals and leveraging the strong semantic capability of VLMs, OmniGF seamlessly integrates precise spatial gaze target estimation, semantic gaze prediction, and complex social gaze reasoning. Extensive experiments demonstrate that our framework establishes new state-of-the-art performance across multiple standard benchmarks. Code is available at <https://github.com/cvlab-stonybrook/omnigf>.

## 1 Introduction

Gaze following, which aims to infer where a person is looking within a scene, is a fundamental component of human social cognition and a critical task in computer vision. Accurately estimating human gaze targets is essential for a wide array of downstream applications, including human-robot interaction [1–3], autonomous driving [4–6], social behavioral analysis [7, 8], and the diagnosis of neurodevelopmental disorders [9, 10]. Historically, the field has been dominated by specialized Convolutional Neural Networks (CNNs) [11–14] and Vision Transformers (ViTs) [15, 16]. While effective for basic spatial localization, these traditional models often process individuals sequentially, requiring redundant processing of the same scene image to predict gaze targets for multiple individuals. Furthermore, most methods are limited to pure spatial localization, lacking the high-level capacity to reason about the target semantics or to understand the broader context of human social interactions.

Recently, large Vision-Language Models (VLMs) have demonstrated unprecedented capabilities in generalized visual reasoning, achieving remarkable success across a variety of zero-shot and downstream tasks related to semantic reasoning, such as referring expression comprehension [17] and semantic segmentation [18, 19]. However, trivially applying off-the-shelf VLMs to gaze following

yields clearly suboptimal performance. Standard VLMs represent spatial coordinates using discrete language tokens, a paradigm that is inherently misaligned with the continuous, high-resolution precision required for dense spatial tasks like gaze localization. While a few pioneering works have attempted to bridge this gap, they remain limited. For instance, GazeVLM [20] relies on auxiliary depth map inputs yet fails to achieve competitive spatial precision against state-of-the-art vision-only models. Similarly, VL4Gaze [21] predominantly focuses on Gaze-oriented Visual Question Answering (VQA) and does not comprehensively address or evaluate standard 2D spatial gaze following benchmarks. Consequently, effectively harnessing the semantic power of VLMs for precise, multi-person gaze localization remains an open challenge.

To overcome these limitations, we propose OmniGF, a novel, unified Vision-Language framework for multi-person gaze target estimation and reasoning. Instead of forcing a VLM to regress spatial coordinates purely through discrete text tokens, we introduce a dual-branch decoding architecture. Our framework utilizes a fine-tuned structured language branch to generate discrete reasoning states (e.g., 2D target location, target in/out of frame, and semantic category), while simultaneously employing a continuous gaze branch dedicated to the dense spatial decoding of target heatmaps. This spatial decoder dynamically taps into the VLM’s hidden state tokens derived from the generated gaze-related text for each person. By associating the visual embeddings of the scene with the gaze representations from the hidden states for each person, the model predicts gaze target heatmaps that directly benefit from the dense supervision signals, significantly improving spatial localization performance.

Furthermore, to ensure more efficient processing of complex scenes, OmniGF models multiple individuals jointly. To explicitly ground the VLM to each specific individual, we introduce a head-conditioned token injection mechanism. By embedding cropped visual head features directly into dedicated prompt token slots, we provide the backbone with the fine-grained appearance and orientation cues necessary to accurately disambiguate targets in dense environments. Crucially, by leveraging the strong semantic reasoning capacity of the VLM backbone, our framework seamlessly extends beyond simple coordinate regression. OmniGF jointly supports auxiliary tasks such as semantic gaze target recognition (identifying *what* object is being looked at) and pairwise social gaze reasoning (e.g., shared attention and mutual gaze), unifying spatial, semantic, and social gaze understanding within a single model.

In summary, our main contributions are as follows:

- **Unified Multi-Person VLM Framework.** We introduce OmniGF, a person-aware vision-language framework that models multiple individuals jointly via structured prompts, processing all persons together from a single VLM input.
- **Head-Conditioned Token Injection.** We propose a simple yet effective mechanism that injects head-centric visual embeddings into dedicated token slots, grounding the VLM with fine-grained appearance and orientation cues for each individual.
- **Dual-Branch Decoding for Reasoning and Spatial Prediction.** We design a dual-branch architecture that combines structured language generation for discrete reasoning with a gaze branch that extracts hidden states to predict dense, high-resolution gaze heatmaps.
- **Unified Gaze, Semantic, and Social Understanding.** Our framework jointly supports gaze target estimation, semantic gaze prediction, and pairwise social gaze reasoning within a single model, achieving state-of-the-art performance across five different benchmarks.

## 2 Related Works

**Gaze Following** aims to predict the location where a person is looking in a scene image. Early methods mostly adopted a two-branch design for gaze target prediction, with one branch encoding head pose and appearance and the other encoding scene saliency information [11, 22, 12, 23]. Later works leveraged additional modalities, such as depth and human pose, to further improve model performance [13, 24, 14, 25–29]. More recent models have incorporated large pretrained foundation models and achieved impressive performance on gaze following. Sharingan [15] uses Multi-MAE [30] for multi-person gaze following, while Gaze-LLE [16] employs DINOv2 [31] with a head-prompting strategy and achieves further improvements. In parallel, several works have addressed gaze following from different perspectives, such as jointly predicting subject heads and their corresponding gaze targets [32–34], incorporating audio cues for gaze following [35], or estimating gaze targets from

multiple camera views [36]. Meanwhile, recent works have explored jointly solving additional tasks together with gaze target estimation. Tafasca et al. [37] explored joint prediction of the location and semantic label of the gaze target, while Gupta et al. [38] studied joint gaze target estimation and social gaze prediction. In this paper, we explore the use of multimodal LLMs for gaze target estimation and show that they can be seamlessly extended to semantic and social gaze prediction tasks as well.

**Vision-Language Models** (VLMs) like LLaVA [39] and the Qwen-VL series [40–42] excel at generalized visual reasoning and have been successfully adapted for dense downstream tasks like visual grounding [43] and segmentation [18, 19, 44]. However, their direct application to gaze following remains limited. Prior works primarily utilize VLMs for auxiliary purposes, such as extracting zero-shot contextual embeddings used for existing vision-based models [45] or generating pseudo-annotations [46], rather than for direct localization. Concurrent VLM-based gaze models also exhibit notable limitations: GazeVLM [20] relies on auxiliary depth inputs and lags behind specialized spatial models in precision, while VL4Gaze [21] formulates the problem purely as VQA rather than evaluating on standard spatial localization benchmarks. In contrast, our work directly adapts VLMs for standard gaze target estimation, demonstrating state-of-the-art effectiveness across continuous spatial localization, semantic prediction, and complex social gaze reasoning.

### 3 Method

Given an input image  $I \in \mathbb{R}^{H \times W \times 3}$  and a set of  $N$  head bounding boxes  $\mathcal{B} = \{b_i\}_{i=1}^N$ , where  $b_i \in \mathbb{R}^4$  denotes the head region of person  $P_i$ , our primary objective is to predict each person’s gaze status (whether the target is inside or outside the frame) and to estimate the precise target coordinates if it falls within the image (*where*). Furthermore, our framework seamlessly extends to higher-level relational tasks. For Semantic Gaze Reasoning, we infer the categorical identity of the object being attended to by each individual (*what*). For Social Gaze Interaction, we analyze every pair of individuals ( $P_i, P_j$ ) to classify their relational dynamics into three distinct categories: Looking At Humans (LAH), Looking At Each Other (LAEO), and Shared Attention (SA).

#### 3.1 Overview

Our framework is built upon a LoRA-tuned Qwen3-VL [42] backbone that processes the image, system instruction prompt (see Appendix for complete descriptions), and structured multi-person prompts as input, where visual head embeddings are dynamically injected into the token sequence to ground each subject (Sec. 3.2). The architecture features a Structured Language Branch (Sec. 3.2.1), which leverages the VLM’s discrete reasoning capacity to generate per-person textual predictions  $\hat{T}_i$  including gaze status, coordinates, and semantic categories, and a Gaze Branch (Sec. 3.2.2), which decodes dense spatial signals from the backbone’s hidden states to output high-resolution gaze heatmaps  $M_i \in \mathbb{R}^{H' \times W'}$ , along with binary in/out logits  $p_i^{in}$ , and pairwise social gaze logits  $S_{i,j} \in \mathbb{R}^3$  from different prediction heads. By tapping into subject-specific hidden states and supervised with dense spatial heatmaps, this branch provides notably better localization than text-based coordinate generation. Therefore, we utilize the target derived from the dense heatmap  $M_i$  as our final spatial gaze prediction. Fig. 1 presents an overview of our framework.

#### 3.2 Multimodal Input Construction and Gaze Token Injection

Given an input image  $I$  and a set of  $N$  head bounding boxes  $\mathcal{B} = \{b_i\}_{i=1}^N$ , where  $b_i = (x_i^1, y_i^1, x_i^2, y_i^2)$ , we first construct a structured text prompt by defining a dedicated slot  $T_i$  for each person using JSON format:  $P_i: \{ \text{"bbox\_2d"} : [x_i^1, y_i^1, x_i^2, y_i^2] \}$ . In a standard VLM pipeline, the image  $I$  is patchified and encoded by a vision encoder into a sequence of global vision tokens  $H_{vis} \in \mathbb{R}^{V \times D}$ , where  $V$  is the number of image patches and  $D$  is the hidden dimension. Simultaneously, the system instructions and the person prompts  $\mathcal{T} = \{T_i\}_{i=1}^N$  are tokenized and embedded into text tokens  $H_{text}$ . These modalities are concatenated to form the initial sequence of hidden states  $H^{(0)} \in \mathbb{R}^{L \times D}$  (where  $L$  is the total sequence length) before being fed into the VLM transformer blocks.

However, relying solely on this standard formulation presents two challenges for gaze target estimation. First, it forces the VLM to perform complex spatial referencing entirely through discrete text tokens. Second, the global vision tokens  $H_{vis}$  may lack the fine-grained, face-centric appearance and 3D orientation cues necessary to disambiguate gaze directions in complex scenes. To resolve

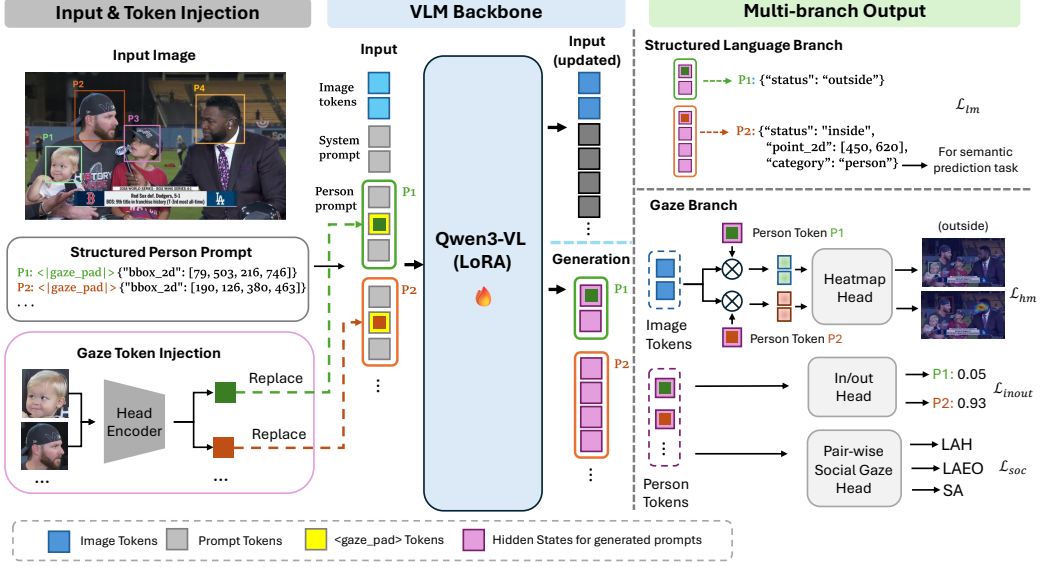


Figure 1: **Overall framework.** Given an image with multiple head bounding boxes, we construct a structured person prompt that assigns each person a  $\langle \text{gaze\_pad} \rangle$  placeholder followed by their head bounding box coordinates. The image, system prompt, and person prompt are processed by a LoRA-tuned Qwen3-VL. During token encoding, each  $\langle \text{gaze\_pad} \rangle$  embedding is replaced with the corresponding head embedding extracted from the cropped head, thereby injecting person-specific visual cues into the VLM. The structured language branch generates JSON outputs for gaze status, target coordinates, and optional semantic categories. The gaze branch extracts image tokens and person tokens from the generated hidden states, where each person token is anchored to the first token of its corresponding generated output sequence. The image and person tokens are combined to predict per-person gaze heatmaps, while the person tokens are further used for in/out prediction and pair-wise social gaze reasoning. For clarity, only two example persons are shown.

this, we introduce a *head-conditioned gaze token injection* mechanism. We augment the input text by prepending a special placeholder token,  $\langle \text{gaze\_pad} \rangle$ , to each person’s prompt entry  $T_i$ :

$$P_i : \langle \text{gaze\_pad} \rangle \{ \text{"bbox\_2d"} : [x_i^1, y_i^1, x_i^2, y_i^2] \}. \quad (1)$$

For each specified box  $b_i$ , we crop the corresponding head region  $c_i$  from the input image  $I$  and process it through a head encoder  $E_{\text{head}}$  to extract a gaze-aware visual embedding  $e_i \in \mathbb{R}^D$ . In our implementation,  $E_{\text{head}}$  utilizes a ResNet-18 backbone [47] pretrained on the Gaze360 dataset [48].

Let  $g_i$  denote the sequence index of the  $\langle \text{gaze\_pad} \rangle$  token associated with person  $P_i$ . Prior to the first transformer layer of the LLM, we replace the text embedding at this index  $H_{g_i}^{(0)}$  with our extracted head embedding  $e_i$ . This targeted substitution explicitly injects localized head appearance and orientation cues into the sequence, grounding the person-specific prompt with rich visual features without disrupting the VLM’s structured multimodal interface.

### 3.2.1 Structured Language Branch

The structured language branch utilizes the standard causal language modeling head of the VLM to autoregressively generate gaze predictions in a parseable JSON format. For each person  $P_i$  specified in the multimodal prompt, the model predicts their gaze status (i.e., whether their gaze target falls inside or outside the image frame). If the target is inside the image, the model outputs the status alongside the normalized 2D target coordinates. For semantic gaze prediction tasks, the model optionally generates a text category describing the gazed-at object.

The generated text  $\hat{T}_i$  for person  $P_i$  follows a strict schema:

$$P_i : \{ \text{"status"} : \text{"inside"}, \text{"point\_2d"} : [x, y], \text{"category"} : \text{"<object>"} \} \quad (2)$$

Conversely, for targets located outside the image frame, the model simplifies the output schema to a single key-value pair: {"status" : "outside"}, omitting any further spatial or semantic attributes.

This text generation provides the discrete inference of the in/out status and the semantic category. Furthermore, the token sequence generated by this branch serves a critical structural purpose: the initial token of the output for each subject (e.g., the "P" token in "P<sub>i</sub> :") acts as a spatial anchor. The hidden states at these specific positions provide person-specific embeddings rich in gaze-aware representations. As detailed in the following section, the gaze branch utilizes these specific token positions to extract person-aligned hidden states for dense geometric prediction. Here, the language branch primarily serves to enforce structured semantic reasoning and establish person-specific token anchors. We supervise the entire JSON text sequence using a standard autoregressive cross-entropy loss  $\mathcal{L}_{lm}$ . However, the 2D gaze target values generated within the text sequence are bypassed in favor of the gaze branch’s dense predictions for the final localization result.

### 3.2.2 Gaze Branch via Hidden State Extraction

While the structured language branch outputs discrete text, continuous geometric and relational predictions are handled by the gaze branch using the model’s internal representations. Specifically, we extract features from the hidden states of the final transformer layer in the VLM, denoted as  $H^{(out)} \in \mathbb{R}^{L' \times D}$ , where  $L'$  corresponds to the total length of the input and generated tokens.

To perform person-specific spatial reasoning, we isolate the hidden state corresponding to the P token in the generated  $P_i$  : for each person as representative person embedding tokens. Because the VLM is instructed to generate personalized gaze information immediately following this token, the hidden state at this specific token position inherently aggregates and encodes rich, gaze-aware features for that individual. We denote this extracted person token as  $h_{p_i} \in \mathbb{R}^{1 \times D}$ . Simultaneously, we extract the sequence of updated image tokens  $H'_{vis} \in \mathbb{R}^{V \times D}$  from  $H^{(out)}$  to serve as the spatial canvas.

These extracted representations are then routed to specialized multi-task heads:

- **Gaze Target Estimation:** To predict the spatial target, the person token  $h_{p_i}$  and the global vision tokens  $H_{vis}$  are fused via element-wise multiplication. This creates a personalized gaze feature for each person, which is then processed by a heatmap decoder consisting of several consecutive transposed convolutional layers to yield a high-resolution gaze target heatmap  $M_i \in \mathbb{R}^{H' \times W'}$  for person  $i$ . This prediction is supervised by the Heatmap Loss  $\mathcal{L}_{hm}$ , which computes the Mean Squared Error (MSE) against a ground-truth heatmap generated by placing a 2D Gaussian distribution at the annotated target coordinate.
- **In/Out Prediction:** The person token  $h_{p_i}$  is passed independently through a Multi-Layer Perceptron (MLP) to output a binary probability logit  $p_i^{in}$ , reinforcing the discrete inside/outside status generated by the language branch. This prediction is supervised by  $\mathcal{L}_{inout}$ , a Binary Cross-Entropy (BCE) loss computed against the ground-truth in/out label.
- **Social Gaze Reasoning:** For complex scene understanding, we evaluate pairwise relational interactions between individuals. For every pair of people  $i$  and  $j$ , we concatenate their respective person tokens to form a joint representation  $[h_{p_i}, h_{p_j}] \in \mathbb{R}^{1 \times 2D}$ . This concatenated feature is passed through a three-layer MLP to estimate independent probability logits  $S_{i,j} \in \mathbb{R}^3$  for three social gaze categories: LAH, LAEO, and SA. We apply a BCE loss independently to each logit to compute the overall Social Gaze Loss  $\mathcal{L}_{soc}$ .

### 3.3 Training Objectives

The entire framework is trained end-to-end in a multi-task manner with LoRA fine-tuning. The overall training objective is defined as a weighted combination of the individual task losses:

$$\mathcal{L}_{total} = \lambda_{lm}\mathcal{L}_{lm} + \lambda_{hm}\mathcal{L}_{hm} + \lambda_{inout}\mathcal{L}_{inout} + \lambda_{soc}\mathcal{L}_{soc} \quad (3)$$

, where  $\lambda_{lm}$ ,  $\lambda_{hm}$ ,  $\lambda_{inout}$ , and  $\lambda_{soc}$  are hyperparameters used to balance the multi-task contributions.

## 4 Experiments

### 4.1 Datasets

We conduct experiments on multiple benchmark datasets, which are described below.

**GazeFollow** [11] is a large-scale image benchmark for gaze following. It comprises around 130K person instances across 122K images. The test set features 4,782 gaze instances, with each target labeled by roughly 10 independent annotators. Furthermore, we utilize the semantic extension introduced by Tafasca et al. [37] for the semantic prediction task, which augments the dataset with target object categories. This extension provides approximately 3,700 pseudo-labels for training and a manually curated test set spanning a 346-class vocabulary for semantic evaluation.

**VideoAttentionTarget** [12] is a video gaze following dataset consisting of 1,331 clips sourced from 50 YouTube TV shows. It provides 164K annotated instances across 71K frames, notably introducing binary inside/outside frame labels for the gaze targets. The test split was constructed by holding out 10 complete TV shows, yielding 31,978 test annotations.

**ChildPlay** [28] is a video dataset focusing on the gaze behaviors of children during social interactions. Sourced from 95 YouTube videos, it yields 401 short clips containing approximately 258K instances across 120K frames. Beyond standard head bounding boxes and 2D target coordinates, instances are annotated with gaze state classes, including target inside, target outside, and gaze shifts, etc.

**GazeHOI** [37] is a benchmark designed for simultaneous spatial localization and semantic classification. Rather than relying on automatically labeled annotations, GazeHOI was constructed by repurposing five established Human-Object Interaction (HOI) datasets, isolating specific interaction verbs where a person’s gaze is directed at the interacted object. The primary evaluation set provides 55,995 gaze instances across 463 distinct object categories.

**VSGaze** [38] is a composite dataset specifically designed for social gaze prediction, aggregating data from VideoAttentionTarget, ChildPlay, VideoCoAtt [49], and UCO-LAEO [50]. The authors unified these disparate sources through a cross-annotation pipeline. First, they generated continuous head track annotations by detecting missing heads and tracking them across frames. Second, they cross-annotated the tasks: social gaze datasets (VideoCoAtt, UCO-LAEO) were augmented with spatial gaze targets approximated at bounding box centers, while the gaze following datasets were extended with social gaze labels. The resulting unified dataset contains 714K annotated gaze points with 444k, 30k, 420k positive pair-wise social gaze labels for LAH, LAEO, and SA respectively.

### 4.2 Evaluation Metrics

For gaze target localization, we compute the L2 distance (**Dist.**) on a normalized  $1 \times 1$  image plane, extracting the predicted coordinate from the peak heatmap activation. To account for multiple annotators in GazeFollow, we report both **Avg Dist.** and **Min Dist.**. Target inside/outside prediction is evaluated via **Average Precision (AP)**.

For semantic gaze prediction on GazeFollow, we report top-1 accuracy (**Accuracy@1**) and **MultiAccuracy@1**, which accounts for multiple labels that can be assigned to the same subject. Because our framework generates text for semantic labels rather than probability logits, we omit **Accuracy@3**. On GazeHOI, we evaluate target localization using **GazeAcc**, which measures whether the predicted point falls within the ground-truth object bounding box, along with **Accuracy@1** for recognition.

For social gaze prediction on VSGaze, we follow the standard pairwise evaluation protocol established by MTGS [38], reporting **F1** scores for LAH and LAEO, and **AP** for SA.

### 4.3 Implementation Details

Our framework utilizes the Qwen3-VL-4B-Instruct backbone, adapted via LoRA ( $r = 16, \alpha = 32$ ). The head bounding box coordinates are normalized to the relative coordinate range  $[0, 1000]$  in the input prompt following the grounding convention of Qwen3-VL. Input resolutions are fixed at  $448 \times 448$  for the global scene and  $224 \times 224$  for cropped heads. We train with a batch size 8 with two gradient accumulation steps using the AdamW optimizer and a cosine annealing scheduler. For training on GazeFollow, we set the learning rate to  $10^{-4}$  for the LoRA adapter and  $2.5 \times 10^{-4}$  for the gaze prediction heads. The models are fine-tuned from this checkpoint using reduced learning

Table 1: Comparison with state-of-the-art methods on GazeFollow and VideoAttentionTarget. In the column of input modality, I is image, D is depth, P is pose, and E is eyes. Best numbers are marked as bold while second-best are underlined.

Method	Input	Multi-person inference support	GazeFollow		VideoAttentionTarget	
			Avg Dist. ↓	Min Dist. ↓	Dist. ↓	AP ↑
Recasens [11]	I	×	0.190	0.113	–	–
Chong [22]	I	×	0.187	0.112	0.171	0.712
Lian [23]	I	×	0.145	0.081	–	–
Chong [12]	I	×	0.137	0.077	0.134	0.853
Fang [13]	I+D+E	×	0.124	0.067	0.108	0.896
Jin [51]	I	✓	0.126	0.076	0.127	0.882
Bao [24]	I+D+P	×	0.122	–	0.120	0.869
Jin [27]	I+D+P	×	0.118	0.063	0.104	0.895
Gupta [14]	I+D+P	×	0.114	0.056	0.110	0.879
Miao [25]	I+D	×	0.123	0.065	0.109	0.908
Tafasca [28]	I+D	×	0.122	0.062	0.109	0.834
Sharingan [15]	I	✓	0.113	0.057	0.107	0.891
MTGS [38]	I	✓	0.116	0.059	0.105	0.869
Gaze-LLE (ViT-B) [16]	I	×	0.104	0.045	0.107	0.897
Gaze-LLE (ViT-L) [16]	I	×	0.099	0.041	0.103	0.903
GazeVLM [20]	I+D	✓	0.123	0.061	0.102	0.898
OmniGF (proposed)	I	✓	<b>0.091</b>	<b>0.040</b>	<b>0.096</b>	<b>0.923</b>
Human	–	–	0.096	0.040	0.051	0.925

rates of  $2.5 \times 10^{-5}$  for VideoAttentionTarget and ChildPlay, and  $10^{-4}$  for VSGaze. The multi-task loss coefficients are empirically set to  $\lambda_{lm} = 1.0$ ,  $\lambda_{hm} = 10.0$ ,  $\lambda_{inout} = 0.1$ , and  $\lambda_{soc} = 1.0$  (when applicable). When training the model for semantic and social gaze prediction task, we fine-tuned the model from the localization-only checkpoint on GazeFollow. Experiments are conducted on an Nvidia H100 GPU (80 GB). Training times vary from 2 to 30 hours across datasets.

#### 4.4 Comparison with State-of-the-Art

We compare our proposed framework against existing state-of-the-art gaze following methods on the GazeFollow and VideoAttentionTarget datasets in Table 1, and on the ChildPlay dataset in Table 2. Our framework establishes a new state-of-the-art across all primary target estimation and in/out prediction metrics on all datasets. On GazeFollow, our method achieves an exceptional Avg Dist. of 0.091 and a Min Dist. of 0.040, notably surpassing even the reported human performance baseline for Avg Dist. (0.096). On VideoAttentionTarget, our model achieves the lowest spatial error (Dist. 0.096) and highly competitive in/out prediction performance (AP 0.923), closing the gap toward human-level recognition. Crucially, our model achieves these results by processing all people with a single VLM input using solely RGB image inputs. This significantly outperforms complex architectures that rely on auxiliary modalities (e.g., depth, pose) and establishes a massive performance margin over prior multi-person capable models (e.g., a 0.022 improvement in Avg Dist. over Sharingan on GazeFollow). Furthermore, our model significantly outperforms GazeVLM, a concurrent VLM-based baseline that requires depth images as an additional input modality. Meanwhile, we validate our model’s robustness on the ChildPlay dataset, where it achieves a new state-of-the-art Dist. of 0.090 and an AP of 0.996, outperforming recent frameworks like Sharingan and Gaze-LLE. Qualitative results in Fig. 2 shows high-quality multi-person gaze predictions from our model across multiple datasets.

#### 4.5 Ablation Study

To validate our architectural innovations, we conduct a comprehensive ablation study on the Gaze-Follow dataset (Table 3). We first evaluate the pretrained Qwen3-VL [42] backbone in a zero-shot setting. Using our exact system and person prompts to instruct the model to generate gaze status and target coordinates in text, it yields very poor localization (0.340 Avg Dist.). This confirms that off-the-shelf text generation struggles with precise spatial localization for gaze following. Fine-tuning the structured language branch via LoRA significantly reduces this error (0.114) but remains limited



Figure 2: Visualizations of model predictions of OmniGF on GazeFollow (1st and 2nd columns), VideoAttentionTarget (3rd column) and ChildPlay (4th column). The first row shows predicted gaze target locations for multiple persons in an image. The 2nd row shows the predicted heatmap for a representative person in the image. Ground truth annotations are visualized in yellow, and the predicted point is visualized in red.

Table 2: Comparison Results on ChildPlay.

Method	Dist. ↓	AP ↑
Gupta [14]	0.113	0.983
Tafasca [28]	0.107	0.986
Sharingan [15]	0.106	0.990
MTGS [38]	0.117	0.993
Gaze-LLE (ViT-B) [16]	0.106	0.994
Gaze-LLE (ViT-L) [16]	0.101	0.994
OmniGF (proposed)	<b>0.090</b>	<b>0.996</b>

Table 3: Ablation Results on GazeFollow.

Components			Metrics	
Language (LoRA)	Spatial Decoding	Token Inject.	Avg ↓	Min ↓
			0.340	0.258
✓			0.114	0.055
	✓		0.167	0.103
✓	✓		0.104	0.047
✓	✓	✓	<b>0.091</b>	<b>0.040</b>

by the precision bottleneck of text-based target localization. Conversely, training only the continuous gaze branch for dense heatmap decoding proves suboptimal (0.167). Because the heatmap head relies on person token embeddings extracted from the prompt, failing to simultaneously fine-tune the language branch deprives these embeddings of the necessary gaze-related context for accurate heatmap prediction. However, combining both approaches into our dual-branch architecture overcomes these limitations (0.104), proving that the hidden state tokens produced during language generation serve as essential structural anchors for extracting high-resolution spatial heatmaps. Finally, integrating dynamic gaze token injection achieves our state-of-the-art performance (0.091 Avg Dist.). By injecting cropped visual head embeddings directly into the input sequence, this mechanism provides the explicit, fine-grained appearance and orientation cues necessary to accurately disambiguate targets.

#### 4.6 Performance on Semantic Gaze Prediction

Beyond standard spatial coordinate estimation, our framework seamlessly extends to semantic gaze target recognition by generating an additional "category" field within the structured language output. Because our model generates open-vocabulary text rather than discrete class logits, predicted labels may not perfectly align with the predefined test vocabulary. To resolve this, we encode both our text predictions and the evaluation classes using CLIP (utilizing the prompt template "a photo of [label]") and assign the closest matching test class via cosine similarity.

Furthermore, we identified noticeable noise in the original pseudo-labeled GazeFollow training set established by Sengaze (e.g., a "cellphone" being hold was incorrectly labeled as "person"). To ensure high-quality supervision, we refined these pseudo-labels and subsequently trained both our model and a corrected Sengaze\* baseline on this improved data. We will publicly release these refined annotations to support future research. Conversely, for GazeHOI, we maintained the original semantic labels because these are derived directly from the ground-truth object bounding boxes of established Human-Object Interaction datasets.

As shown in Tables 4 and 5, OmniGF establishes new state-of-the-art performance on both datasets. On GazeFollow, it achieves a remarkable Acc@1 of 0.649, with a 23.1% improvement over the

Table 4: Semantic gaze prediction results on GazeFollow. Semgaze\* denotes the baseline trained on our refined ground-truth labels for a fair comparison.

Method	Localization		Recognition	
	Avg. Dist. ↓	Min. Dist. ↓	Acc@1 ↑	MultiAcc@1 ↑
Semgaze [37]	0.108	0.051	0.447	0.516
Semgaze* [37]	0.109	0.053	0.527	0.598
OmniGF (proposed)	<b>0.092</b>	<b>0.040</b>	<b>0.649</b>	<b>0.739</b>

Table 5: Semantic gaze prediction on GazeHOI. Semgaze\* is omitted as semantic labels for GazeHOI are derived directly from existing HOI datasets.

Method	Localization	Recognition
	GazeAcc ↑	Acc@1 ↑
Semgaze [37]	0.723	0.583
OmniGF (proposed)	<b>0.786</b>	<b>0.722</b>

corrected SemGaze baseline. Besides, it also excels in both localization and recognition on GazeHOI, outperforming SemGaze by 23.8%. This confirms that our dual-branch VLM architecture effectively bridges the gap between precise spatial localization and high-level semantic reasoning.

#### 4.7 Performance on Social Gaze Prediction

Finally, we extend our framework to the complex task of social gaze prediction using the VSGaze dataset. A unique challenge of this dataset is that it includes additional head bounding boxes and tracks that lack ground-truth gaze target annotations. To effectively train our structured language branch in this dense multi-person environment, we introduce a selective loss masking strategy. Specifically, we input dummy gaze slots for these unannotated individuals and assign them a categorical gaze status of “unknown.” During backpropagation, we dynamically exclude the tokens corresponding to these individuals from the language modeling gradient. This ensures the model learns to process all individuals in the scene simultaneously for global context, while focusing its parameter updates strictly on valid, annotated targets.

As shown in Table 6, our framework establishes a new state-of-the-art across all gaze and social reasoning metrics. Crucially, our model performs end-to-end (E2E) social gaze reasoning jointly with gaze localization, eliminating the need for the manual post-processing required by ordinary gaze following methods. Compared to the only E2E baseline MTGS [38], our model improves from 0.590 to 0.742 (25.8%) on  $F1_{LAE0}$  and from 0.576 to 0.787 (36.6%) on  $AP_{SA}$ . These unprecedented gains demonstrate that leveraging the semantic reasoning capabilities of a VLM provides a fundamental advantage in understanding complex social interactions over traditional spatial-only architectures.

Table 6: Comparison of social gaze reasoning and gaze target estimation performance. E2E denotes end-to-end prediction without relying on manual post-processing heuristics.

Method	E2E	Dist. ↓	$AP_{IO}$ ↑	$F1_{LAH}$ ↑	$F1_{LAE0}$ ↑	$AP_{SA}$ ↑
Chong <sub>S</sub> [12]	×	0.121	0.918	0.778	0.562	0.288
Chong <sub>T</sub> [12]	×	0.130	0.956	0.764	0.529	0.331
Gupta [14]	×	0.119	0.929	0.784	0.590	0.335
MTGS [38]	✓	0.107	0.940	0.795	0.590	0.576
OmniGF (proposed)	✓	<b>0.098</b>	<b>0.992</b>	<b>0.814</b>	<b>0.742</b>	<b>0.787</b>

## 5 Conclusion

In this work, we presented OmniGF, a novel Vision-Language framework for unified gaze following. By introducing a dual-branch architecture that harmonizes a structured language branch with a continuous dense spatial decoder, alongside a dynamic gaze token injection mechanism, we successfully adapted a foundational VLM for high-precision spatial reasoning tasks. OmniGF establishes a new state-of-the-art across diverse benchmarks in a single multi-person forward pass. To the best of our knowledge, this is the first successful application of VLMs to gaze localization that outperforms state-of-the-art vision-based models. Furthermore, benefiting from VLM’s strong semantic reasoning capacity, we demonstrate that the model can be seamlessly extended to semantic and social gaze prediction tasks, outperforming current state-of-the-art models by a significant margin. This demonstrates that foundational VLMs can fundamentally unify spatial localization and discrete high-level semantic reasoning. We hope that OmniGF provides a robust, streamlined foundation to accelerate future research in human behavior understanding, social scene analysis, and interactive AI systems.

## References

- [1] S. Sheikhi and J.-M. Odobez, “Combining dynamic head pose–gaze mapping with the robot conversational state for attention recognition in human–robot interactions,” *Pattern Recognition Letters*, vol. 66, pp. 81–90, 2015.
- [2] H. Admoni and B. Scassellati, “Social eye gaze in human-robot interaction: a review,” *Journal of Human-Robot Interaction*, vol. 6, no. 1, pp. 25–63, 2017.
- [3] A. Saran, S. Majumdar, E. S. Short, A. Thomaz, and S. Niekum, “Human gaze following for human-robot interaction,” in *2018 IEEE/RSJ International Conference on Intelligent Robots and Systems (IROS)*, pp. 8615–8621, IEEE, 2018.
- [4] I. Kasahara, S. Stent, and H. S. Park, “Look both ways: Self-supervising driver gaze estimation and road scene saliency,” in *European Conference on Computer Vision*, pp. 126–142, Springer, 2022.
- [5] S. Martin, S. Vora, K. Yuen, and M. M. Trivedi, “Dynamics of driver’s gaze: Explorations in behavior modeling and maneuver prediction,” *IEEE Transactions on Intelligent Vehicles*, vol. 3, no. 2, pp. 141–150, 2018.
- [6] C. Liu, Y. Chen, L. Tai, H. Ye, M. Liu, and B. E. Shi, “A gaze model improves autonomous driving,” in *Proceedings of the 11th ACM symposium on eye tracking research & applications*, pp. 1–5, 2019.
- [7] N. J. Emery, “The eyes have it: the neuroethology, function and evolution of social gaze,” *Neuroscience & biobehavioral reviews*, vol. 24, no. 6, pp. 581–604, 2000.
- [8] B. Massé, S. Ba, and R. Horaud, “Tracking gaze and visual focus of attention of people involved in social interaction,” *IEEE transactions on pattern analysis and machine intelligence*, vol. 40, no. 11, pp. 2711–2724, 2017.
- [9] A. Senju and M. H. Johnson, “Atypical eye contact in autism: Models, mechanisms and development,” *Neuroscience & Biobehavioral Reviews*, vol. 33, no. 8, pp. 1204–1214, 2009.
- [10] R. A. J. De Belen, T. Bednarz, A. Sowmya, and D. Del Favero, “Computer vision in autism spectrum disorder research: a systematic review of published studies from 2009 to 2019,” *Translational psychiatry*, vol. 10, no. 1, p. 333, 2020.
- [11] A. Recasens, A. Khosla, C. Vondrick, and A. Torralba, “Where are they looking?,” in *Advances in Neural Information Processing Systems* (C. Cortes, N. Lawrence, D. Lee, M. Sugiyama, and R. Garnett, eds.), vol. 28, Curran Associates, Inc., 2015.
- [12] E. Chong, Y. Wang, N. Ruiz, and J. M. Rehg, “Detecting attended visual targets in video,” in *Proceedings of the IEEE/CVF Conference on Computer Vision and Pattern Recognition*, pp. 5396–5406, 2020.
- [13] Y. Fang, J. Tang, W. Shen, W. Shen, X. Gu, L. Song, and G. Zhai, “Dual attention guided gaze target detection in the wild,” in *Proceedings of the IEEE/CVF Conference on Computer Vision and Pattern Recognition*, pp. 11390–11399, 2021.
- [14] A. Gupta, S. Tafasca, and J.-M. Odobez, “A modular multimodal architecture for gaze target prediction: Application to privacy-sensitive settings,” in *Proceedings of the IEEE/CVF Conference on Computer Vision and Pattern Recognition Workshops*, pp. 5041–5050, 2022.
- [15] S. Tafasca, A. Gupta, and J.-M. Odobez, “Sharingan: A transformer architecture for multi-person gaze following,” in *Proceedings of the IEEE/CVF Conference on Computer Vision and Pattern Recognition*, pp. 2008–2017, 2024.
- [16] F. Ryan, A. Bati, S. Lee, D. Bolya, J. Hoffman, and J. M. Rehg, “Gaze-llc: Gaze target estimation via large-scale learned encoders,” in *Proceedings of the Computer Vision and Pattern Recognition Conference*, pp. 28874–28884, 2025.
- [17] K. Chen, Z. Zhang, W. Zeng, R. Zhang, F. Zhu, and R. Zhao, “Shikra: Unleashing multimodal LLM’s referential dialogue magic,” *arXiv preprint arXiv:2306.15195*, 2023.
- [18] L. Beyer, A. Steiner, A. S. Pinto, A. Kolesnikov, X. Wang, D. Salz, M. Neumann, I. Alabdulmohsin, M. Tschanen, E. Bugliarello, T. Unterthiner, D. Keysers, S. Koppula, F. Liu, A. Grycner, A. Gritsenko, N. Houlsby, M. Kumar, K. Rong, J. Eisenschlos, R. Kabra, M. Bauer, M. Bošnjak, X. Chen, M. Minderer, P. Voigtlaender, I. Bica, I. Balazevic, J. Puigcerver, P. Papalampidi, O. Henaff, X. Xiong, R. Soricut, J. Harmsen, and X. Zhai, “PaliGemma: A versatile 3b VLM for transfer,” *arXiv preprint arXiv:2407.07726*, 2024.

- [19] L. H. Li, P. Zhang, H. Zhang, J. Yang, C. Li, Y. Zhong, L. Wang, L. Yuan, L. Zhang, J.-N. Hwang, K.-W. Chang, and J. Gao, “Grounded language-image pre-training,” in *Proceedings of the IEEE/CVF Conference on Computer Vision and Pattern Recognition (CVPR)*, 2022.
- [20] A. M. Mathew, H. Hermassi, T. Khalid, and A. A. Khan, “GazeVLM: A vision-language model for multi-task gaze understanding,” *arXiv preprint arXiv:2511.06348*, 2025.
- [21] S. Wang, C. Cui, Y. Huang, H. J. Chang, and Y. Cheng, “VL4Gaze: Unleashing vision-language models for gaze following,” *arXiv preprint arXiv:2512.20735*, 2025.
- [22] E. Chong, N. Ruiz, Y. Wang, Y. Zhang, A. Rozga, and J. M. Rehg, “Connecting gaze, scene, and attention: Generalized attention estimation via joint modeling of gaze and scene saliency,” in *Proceedings of the European Conference on Computer Vision*, pp. 383–398, 2018.
- [23] D. Lian, Z. Yu, and S. Gao, “Believe it or not, we know what you are looking at!,” in *Proceedings of the Asian Conference on Computer Vision*, pp. 35–50, Springer, 2018.
- [24] J. Bao, B. Liu, and J. Yu, “Escnet: Gaze target detection with the understanding of 3d scenes,” in *Proceedings of the IEEE/CVF Conference on Computer Vision and Pattern Recognition*, pp. 14126–14135, June 2022.
- [25] Q. Miao, M. Hoai, and D. Samaras, “Patch-level gaze distribution prediction for gaze following,” in *Proceedings of the IEEE/CVF Winter Conference on Applications of Computer Vision*, pp. 880–889, 2023.
- [26] Z. Hu, D. Yang, S. Cheng, L. Zhou, S. Wu, and J. Liu, “We know where they are looking at from the rgb-d camera: Gaze following in 3d,” *IEEE Transactions on Instrumentation and Measurement*, vol. 71, pp. 1–14, 2022.
- [27] T. Jin, Q. Yu, S. Zhu, Z. Lin, J. Ren, Y. Zhou, and W. Song, “Depth-aware gaze-following via auxiliary networks for robotics,” *Engineering Applications of Artificial Intelligence*, vol. 113, p. 104924, 2022.
- [28] S. Tafasca, A. Gupta, and J.-M. Odobez, “Childplay: A new benchmark for understanding children’s gaze behaviour,” in *Proceedings of the IEEE/CVF International Conference on Computer Vision*, pp. 20935–20946, 2023.
- [29] Y. Yang, Y. Yin, and F. Lu, “Gaze target detection by merging human attention and activity cues,” in *Proceedings of AAAI Conference on Artificial Intelligence*, vol. 38, pp. 6585–6593, 2024.
- [30] R. Bachmann, D. Mizrahi, A. Atanov, and A. Zamir, “Multimae: Multi-modal multi-task masked autoencoders,” in *Proceedings of the European Conference on Computer Vision*, pp. 348–367, Springer, 2022.
- [31] M. Oquab, T. Darcet, T. Moutakanni, H. Vo, M. Szafraniec, V. Khalidov, P. Fernandez, D. Haziza, F. Massa, A. El-Nouby, *et al.*, “Dinov2: Learning robust visual features without supervision,” *arXiv preprint arXiv:2304.07193*, 2023.
- [32] D. Tu, X. Min, H. Duan, G. Guo, G. Zhai, and W. Shen, “End-to-end human-gaze-target detection with transformers,” in *Proceedings of the IEEE/CVF Conference on Computer Vision and Pattern Recognition*, pp. 2192–2200, IEEE, 2022.
- [33] F. Tonini, N. Dall’Asen, C. Beyan, and E. Ricci, “Object-aware gaze target detection,” in *Proceedings of the IEEE/CVF International Conference on Computer Vision*, pp. 21860–21869, 2023.
- [34] D. Tu, W. Shen, W. Sun, X. Min, and G. Zhai, “Joint gaze-location and gaze-object detection,” *arXiv preprint arXiv:2308.13857*, 2023.
- [35] Y. Hou, Z. Zhang, N. Horanyi, J. Moon, Y. Cheng, and H. J. Chang, “Multi-modal gaze following in conversational scenarios,” in *Proceedings of the IEEE/CVF Winter Conference on Applications of Computer Vision*, pp. 1186–1195, 2024.
- [36] Q. Miao, V. R. Golani, J. Xu, P. P. Dutta, M. Hoai, and D. Samaras, “Multi-view gaze target estimation,” in *Proceedings of the IEEE/CVF International Conference on Computer Vision*, pp. 5371–5381, 2025.
- [37] S. Tafasca, A. Gupta, V. Bros, and J.-M. Odobez, “Toward semantic gaze target detection,” *Advances in neural information processing systems*, vol. 37, pp. 121422–121448, 2024.
- [38] A. Gupta, S. Tafasca, A. Farkhondeh, P. Vuillecard, and J. marc Odobez, “MTGS: A novel framework for multi-person temporal gaze following and social gaze prediction,” in *Advances in Neural Information Processing Systems*, 2024.

- [39] H. Liu, C. Li, Q. Wu, and Y. J. Lee, “Visual instruction tuning,” in *Advances in Neural Information Processing Systems*, vol. 36, 2023.
- [40] J. Bai, S. Bai, S. Yang, S. Wang, S. Tan, P. Wang, J. Lin, C. Zhou, and J. Zhou, “Qwen-VL: A versatile vision-language model for understanding, localization, text reading, and beyond,” *arXiv preprint arXiv:2308.12966*, 2023.
- [41] P. Wang, S. Bai, S. Tan, S. Wang, Z. Fan, J. Bai, K. Chen, X. Liu, J. Wang, W. Ge, *et al.*, “Qwen2-vl: Enhancing vision-language model’s perception of the world at any resolution,” *arXiv preprint arXiv:2409.12191*, 2024.
- [42] S. Bai, Y. Cai, R. Chen, K. Chen, X. Chen, Z. Cheng, L. Deng, W. Ding, C. Gao, C. Ge, *et al.*, “Qwen3-vl technical report,” *arXiv preprint arXiv:2511.21631*, 2025.
- [43] H. Rasheed, M. Maaz, S. Shaji, A. Shaker, S. Khan, H. Cholakkal, R. M. Anwer, E. Xing, M.-H. Yang, and F. S. Khan, “GLaMM: Pixel grounding large multimodal model,” in *Proceedings of the IEEE/CVF Conference on Computer Vision and Pattern Recognition (CVPR)*, June 2024.
- [44] X. Lai, Z. Tian, Y. Chen, Y. Li, Y. Yuan, S. Liu, and J. Jia, “LISA: Reasoning segmentation via large language model,” in *Proceedings of the IEEE/CVF Conference on Computer Vision and Pattern Recognition (CVPR)*, pp. 9579–9589, June 2024.
- [45] A. Gupta, P. Vuillecard, A. Farkhondeh, and J.-M. Odobez, “Exploring the zero-shot capabilities of vision-language models for improving gaze following,” in *Proceedings of the IEEE/CVF Conference on Computer Vision and Pattern Recognition Workshops (CVPRW)*, 2024.
- [46] Q. Miao, A. Graikos, J. Zhang, S. Mondal, M. Hoai, and D. Samaras, “Diffusion-refined VQA annotations for semi-supervised gaze following,” in *European Conference on Computer Vision (ECCV)*, 2024.
- [47] K. He, X. Zhang, S. Ren, and J. Sun, “Deep residual learning for image recognition,” in *Proceedings of the IEEE/CVF Conference on Computer Vision and Pattern Recognition*, pp. 770–778, 2016.
- [48] P. Kellnhofer, A. Recasens, S. Stent, W. Matusik, and A. Torralba, “Gaze360: Physically unconstrained gaze estimation in the wild,” in *Proceedings of the IEEE/CVF International Conference on Computer Vision*, pp. 6912–6921, 2019.
- [49] L. Fan, Y. Chen, P. Wei, W. Wang, and S.-C. Zhu, “Inferring shared attention in social scene videos,” in *Proceedings of the IEEE conference on computer vision and pattern recognition*, pp. 6460–6468, 2018.
- [50] M. J. Marin-Jimenez, V. Kalogeiton, P. Medina-Suarez, and A. Zisserman, “Laeo-net: revisiting people looking at each other in videos,” in *Proceedings of the IEEE/CVF conference on computer vision and pattern recognition*, pp. 3477–3485, 2019.
- [51] T. Jin, Z. Lin, S. Zhu, W. Wang, and S. Hu, “Multi-person gaze-following with numerical coordinate regression,” in *2021 16th IEEE International Conference on Automatic Face and Gesture Recognition (FG 2021)*, pp. 01–08, IEEE, 2021.

## A System Prompts

To effectively guide the Vision-Language Model (VLM) backbone to generate structured reasoning states, we utilize specific system prompts during both training and inference. These prompts inform the model of the input format, establish a normalized coordinate space, and strictly dictate the JSON schema of the desired output.

**Basic Gaze Target Estimation.** For standard spatial gaze target estimation, we use the following base system prompt:

*"You are given an image with head bounding boxes for all people in the scene. Each person is identified as P0..PN with their head box given as {"bbox\_2d": [x1, y1, x2, y2]} in coordinates [0, 999]. For each person, predict whether their gaze target is inside or outside the image. Output one JSON object per person. If the gaze target is inside, output {"status": "inside", "point\_2d": [x, y]}. If outside, output {"status": "outside"}."*

**Semantic Gaze Prediction.** For the semantic gaze target recognition task (evaluated on GazeFollow and GazeHOI), we extend the base prompt to simultaneously reason for the gaze target semantics. We achieve this by appending an instruction to predict what the person is looking at and updating the required JSON schema for in-frame targets. The full system prompt is formulated as follows:

*"You are given an image with head bounding boxes for all people in the scene. Each person is identified as P0..PN with their head box given as {"bbox\_2d": [x1, y1, x2, y2]} in coordinates [0, 999]. For each person, predict whether their gaze target is inside or outside the image, and what they are looking at. Output one JSON object per person. If the gaze target is inside, output {"status": "inside", "point\_2d": [x, y], "category": "<object>"}. If outside, output {"status": "outside"}."*

## B Qualitative Results on Auxiliary Tasks

In this section, we present qualitative visualizations across two extended gaze-following tasks: semantic gaze prediction and social gaze prediction.

In Fig. 3, we visualize the predicted gaze targets alongside their predicted semantic labels on the GazeFollow and GazeHOI datasets. As demonstrated, our model accurately localizes the spatial coordinate of the gaze target while simultaneously predicting highly context-aware semantic labels.

In Fig. 4, we illustrate the predicted social gaze labels across diverse interaction scenarios in the VSGaze dataset. The visualizations demonstrate the model’s capacity to robustly predict multi-person social gaze dynamics and complex inter-subject gaze relationships across various challenging sub-datasets.

## C Limitations and Future Work

While OmniGF establishes state-of-the-art performance across multiple benchmarks, we acknowledge a few limitations that provide avenues for future research. First, although our framework achieves single-pass multi-person inference, its reliance on a foundational VLM backbone inherently demands a larger memory footprint and computational budget compared to legacy CNN-based architectures. Future deployments on edge devices could benefit from model quantization or distillation. Second, OmniGF is fundamentally an image-based architecture. When evaluated on video datasets (such as VideoAttentionTarget and ChildPlay), it processes scenes strictly on a frame-by-frame basis without explicit temporal modeling. While it cannot currently leverage motion cues or temporal smoothing to resolve highly ambiguous dynamic gaze behaviors, it is noteworthy that our frame-level approach still outperforms prior methods that explicitly incorporate temporal fusion. Future extensions could investigate on integrating temporal information to further boost robustness in video domains. Finally, while our dynamic gaze token injection scales elegantly to multi-person scenes, localization performance can experience minor drops in extremely crowded environments (e.g., scenes with over 15 individuals in VSGaze). In such extreme cases, the extended input token sequence may lead to attention dilution. Nevertheless, our single-pass mechanism remains vastly more scalable and efficient than the iterative, person-by-person processing required by prior multi-branch architectures.

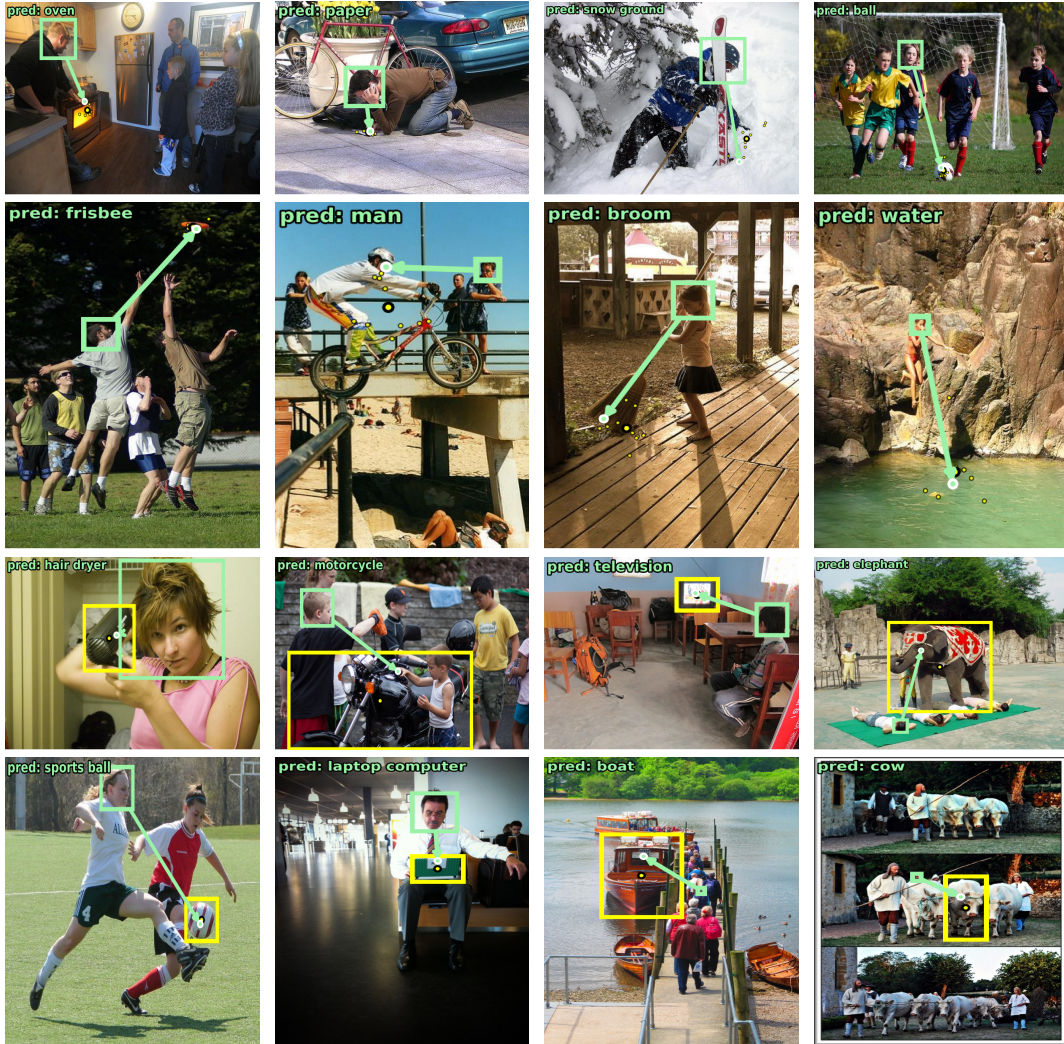


Figure 3: Visualizations of the model predictions with semantic gaze labels on GazeFollow (first two rows) and GazeHOI (last two rows). Yellow dots or bounding boxes indicate the ground truth gaze target. Note that the GazeHOI dataset marks the ground truth gaze target coordinate as the bounding box center of the gaze target object.

## D Broader Impacts

Our proposed framework, OmniGF, advances the capabilities of Vision-Language Models in understanding human gaze and complex social interactions. On the positive side, high-precision gaze estimation holds significant potential for beneficial applications, such as developing more intuitive human-computer interfaces, enabling socially aware collaborative robotics, and providing assistive technologies for individuals with disabilities. Furthermore, it can serve as a valuable analytical tool for behavioral research in psychology and healthcare, potentially aiding in the study of neurodevelopmental conditions such as autism. However, we also acknowledge the potential negative societal impacts of this technology. The ability to accurately track and analyze where individuals are looking in dense, multi-person scenes raises privacy concerns. If deployed irresponsibly, such systems could be misused for intrusive public surveillance, non-consensual tracking of consumer attention in retail environments, or pervasive employee monitoring. Additionally, because our method relies on foundational VLMs, it may inherit or amplify underlying biases present in the large-scale pre-training data, which could lead to disparate performance across different demographic groups.



Figure 4: Qualitative results of social gaze predictions on the VSGaze dataset. Each row presents examples from a constituent sub-dataset: VideoAttentionTarget (Row 1), ChildPlay (Row 2), UCO-LAEO (Row 3), and VideoCoAtt (Row 4). Pairs engaging in Looking At Each Other (LAEO) are connected by solid blue lines, while individuals exhibiting Shared Attention (SA) are connected by dashed purple lines.

We encourage the community to establish strict ethical guidelines and prioritize privacy-preserving mechanisms when deploying gaze-aware systems in real-world environments.